Active control of Boundary Layer Separation & Flow Distortion in Adverse Pressure Gradient Flows via Supersonic Microjets

Final Report
NASA Grant Number: NAG1-01057

Submitted to:
Susan Gorton, Technical Monitor
Flow Physics and Control Branch
NASA Langley Research Center
Mail Stop 170
Hampton, VA 23681

Farrukh S. Alvi
Principal Investigator
Associate Professor
The Department of Mechanical Engineering
FAMU-FSU College of Engineering
Florida A & M University
Tallahassee, FL 32310

Executive Summary

Inlets to aircraft propulsion systems must supply flow to the compressor with minimal pressure loss, flow distortion or unsteadiness. Flow separation in internal flows such as inlets and ducts in aircraft propulsion systems and external flows such as over aircraft wings, is undesirable as it reduces the overall system performance. The aim of this research has been to understand the nature of separation and more importantly, to explore techniques to actively control this flow separation. In particular, the use of supersonic microjets as a means of controlling boundary layer separation was explored. The geometry used for the early part of this study was a simple diverging 'Stratford' ramp, equipped with arrays of supersonic microjets. Initial results, based on the mean surface pressure distribution, surface flow visualization and Planar Laser Scattering (PLS) indicated a reverse flow region. We implemented supersonic microjets to control this separation and flow visualization results appeared to suggest that microjets have a favorable effect, at least to a certain extent. However, the details of the separated flow field were difficult to determine based on surface pressure distribution, surface flow patterns and PLS alone. It was also difficult to clearly determine the exact influence of the supersonic microjets on this flow.

In the latter part of this study, the properties of this flow-field and the effect of supersonic microjets on its behavior were investigated in further detail using 2-component (planar) Particle Image Velocimetry (PIV). The results clearly show that the activation of microjets eliminated flow separation and resulted in a significant increase in the momentum of the fluid near the ramp surface. Also notable is the fact that the gain in momentum due to the elimination of flow separation is at least an order of magnitude larger (two orders of magnitude larger in most cases) than the momentum injected by the microjets and is accomplished with very little mass flow through the microjets.

A new model was subsequently designed where the magnitude and extent of separation could be controlled and also the effect of microjet control could be examined over a wide parametric range. As the results presented in the latter portion of this report will show, microjets were successfully used to control the separation of a much larger extent and magnitude. This study also demonstrated that the microjet parameters could be optimized to reduce the mass requirements significantly, while allowing for effective separation control. Consequently, one of the main outcomes of this research program is a clear demonstration of the significant potential of using microjets for separation control in practical applications.

1. Introduction

Boundary Layer separation entails significant energy loss, increases the flow unsteadiness and limits the performance of many flow devices. Design of engine inlets is one area where prevention of flow separation may be significant in improving the overall efficiency of the vehicle. Flow separation can be prevented in engine inlets by increasing the inlet length which generates a more gradual pressure gradient. However, the increase in the inlet length required to avoid separation and its associated losses may increase the size of the overall vehicle[1]. In addition, for certain military applications, the inlet design is also constrained by low observability requirements. More commonly, a serpentine inlet is used to block the line of sight[2, 3] to the compressor face, thereby reducing the radar signature from the compressor face. Similar "buried" propulsion systems have also been considered for the Blended Wing Body (BWB) design[4].

In case of BWB, the engines are located at the aft end of the aircraft and hence require the ingestion of a thick boundary layer developed over the aircraft surface. The degraded condition of this boundary layer makes it much more susceptible to separation when it encounters the pressure gradients of a diffusing inlet duct. The pressure loss due to this separation reduces the overall system efficiency. Moreover, flow distortion and unsteadiness created due to this separation can also result in aerodynamic stall and surge in the compressor and fan blades[5, 6]. Consequently, it is highly desirable to avoid boundary layer separation in inlets as it can significantly diminish the engine performance.

Not surprisingly, a substantial amount of research aimed at controlling boundary layer separation[7, 8] has been conducted. Conventionally, the following approaches have been applied for separation control: 1) Tangential blowing to directly energize the low momentum region near the wall[9-11], 2) Wall suction[12,13] to remove the low momentum region, 3) Vortex generators (v.g's and micro v.g.'s) in the form of vanes and bumps[14,15], 4) Forced excitation devices e.g. acoustic excitation[16,17] and synthetic jets[18,19]. Tangential blowing and suction are very effective in controlling separation. However, they have the parasitic cost involving high-pressure (mass flux) sources and are infrequently used. Vortex generators are among the most widely examined flow control methods, where v.g.'s of various shapes and sizes have been used to control boundary layer separation[15]. Although the mechanism is still not well understood, it has been suggested that the v.g.'s produce strong vortices, which enhance the mixing between the high momentum core flow and the low momentum boundary layer flow, thus energizing the boundary layer fluid[1]. However, the performance of these v.g.'s, which are passive in nature, has been somewhat limited; usually there is a need to optimize their location, size and other parameters to achieve optimal performance for specific operating conditions. In addition, they have an associated parasitic drag when they are not in use.

An excellent review of active flow control techniques has been published by Greenblatt and Wygnanski[20]. As discussed in their review of the use of acoustic excitation methods for separation control (over airfoils), §3.2 in reference 20, they note that certain methods, such as those used by Ahuja et. al[17] and Zaman et. al[16] have shown some benefits. However, these acoustic excitation studies were in most cases facility dependant and therefore perhaps of limited use from a practical perspective. To quote Greenblatt and Wygnanski (pp. 492) "The drawbacks, however, outweigh these positive aspects". Other active flow control devices, such as synthetic jets[18] have also been examined for separation control applications. Amitay et al.[18] demonstrate that their synthetic jet-based actuators provided some control of flow separation in a duct. The measurements of Amitay et al consisted of pitot surveys which showed that flow attachment was generally obtained for a limited region of the flowfield and complete reattachment was limited to a few cases. Similar flow control devices have been employed by Jenkins et al[19] who employed piezoelectric-synthetic jets to control flow separation over an adverse pressure gradient ramp essentially identical to the one used in the present study. Based on their results, Jenkins et al. conclude that their synthetic jets did not work, primarily due to "insufficient velocity/momentum output" which is needed to achieve effective control.

A different approach, one which employs microjets to control flow separation, has been presented in this paper. In this study, we plan to investigate the efficacy of using high-speed, supersonic for most applications, microjets to control flow separation. Based on their success in other applications[21] and the fact that supersonic microjets provide a unique combination of high momentum and low mass flow rates, we anticipated that these active flow control devices may also be effective in separation control. It is well-known that jets in crossflow, which is in essence the flow generated by the actuation of microjets, can generate longitudinal streamwise vortices[22] in a boundary layer. These vortices in turn appear to increase cross-stream mixing thus increasing the streamwise momentum of the near-wall fluid. It was our expectation, that in a manner similar to solid vortex generators (but perhaps more efficiently), high-speed microjets would thus energize the boundary layer fluid by creating strong streamwise vorticity[23], thereby enhancing mixing with the more energetic flow. Furthermore, due to their small size, relative simplicity and ease of implementation, if successful, engine inlets or other flow surfaces, such as airfoils, can be relatively easily populated with these microjets.

2. Experimental Details

The experiments were conducted in a subsonic, closed return, wind tunnel with a maximum freestream velocity of 65m/s in the 48”x24” test section. A Pitot static probe was used for measuring the inlet flow speed of the wind tunnel. The initial geometry used for the test model was a simple adverse pressure gradient ramp, similar to model used at the NASA Langley Research Center for examining the effectiveness of various control techniques[19]. This geometry produces a Stratford like pressure gradient[24] in the test section. A picture of this model, mounted in the wind tunnel, is shown in Fig. 1. The pressure distribution in the test section is determined from the surface pressure measurements made along the ramp. This ramp is equipped with approximately 50 surface static pressure ports to obtain mean pressure distributions. The pressure ports were placed along the model centerline, as well as in transverse rows at selected locations. The pressure coefficient, C_p, is then determined using the conventional definition

$$C_p = \frac{(P_{surface} - P_{static})}{0.5\rho U_\infty^2}$$

A schematic of this ramp is also shown in Fig. 2. As shown in the figure, the ramp begins at X=0″ and is preceded by a flat region of 21.5″. The figure also indicates the region where the PIV measurements, discussed later in this report, were obtained. As shown in this figure, PIV data was obtained at two longitudinal planes, along the centerline and 0.1S away form the centerline, where S is the span of the ramp. This off-centerline plane is referred to as the “0.4S” location. Also, shown in the figure are the locations of microjets, where only the 1st and 3rd array of microjets were used for control purposes. Each row consists of about 60 microjets, 400μm in diameter. The microjets were oriented vertically, i.e. 90° with respect to the free-stream. The placement of these microjets with respect to separation location is expected to be a critical parameter for the control scheme. It was also anticipated that the actuators should be placed upstream of the separation zone for maximum effect. Since the exact location of the separation was not known, the microjets were placed upstream of the region where separation was observed in the NASA study[19]. The supply to these microjets was made using compressed nitrogen tanks.

Nitrogen was used because it is easily available in pure form and has essentially the same gas dynamic properties as air.

3. Results

Experiments were conducted over an extended range of freestream velocities of 10m/s to 65m/s. For all of these freestream velocities, various combinations of microjet location and pressure were studied. However, for the sake of brevity, unless otherwise stated, results discussed here are mainly limited to 40m/s, as it illustrates the principal flow features and its response to microjet control. The Reynolds number at the ramp leading edge at 40m/s is 1.256×10^6. At this velocity, the boundary layer thickness, δ was measured at the leading edge at the centerline (using a boundary layer pitot probe) and was found to be 0.75 inches. The boundary-layer profile was in close agreement with seventh power law profile indicating that the incoming boundary layer is nominally turbulent. Under these conditions, the corresponding displacement thickness, δ^* and the momentum thickness, θ at the ramp leading edge were estimated to be 0.12″ and 0.08″, respectively.

3.1 Surface Properties: Pressure Distribution

Fig. 3 shows a comparison between the measured C_p distributions for the baseline, uncontrolled flow at 40m/s and flow with microjet control, where the first microjet array (MJ1) has been activated at 25psig. As shown in figure, C_p values have been plotted on a reverse scale on the y-axis. For reference, the ramp geometry is also included, where the ramp height is indicated on the y-axis on the right and the location of the first and the last array of microjets is shown in dashed lines. The repeatability of these experiments was checked over a period of four months and the results were found to be repeatable within 1%. It is observed that upstream of the microjet location, the baseline and the microjet control cases show a similar pressure distribution. Downstream of the microjet location, however, the pressure distributions differ, the pressure recovery being higher for the control case. Similar observations for C_p distributions were made by Lin[15] in his study of separation control using passive control devices. Although the pressure recovery is improved with microjet control, the improvement does not seem to be substantial. As the following results will show, this may partially be because for this case the size of the separation is somewhat limited. Hence the pressure loss will be correspondingly small resulting in a corresponding small recovery when separation is eliminated. Pressure distribution along the centerline, however, provides only limited insight into the flow behavior and based on

C_p distribution alone, it is difficult to conclusively determine whether the effect of microjets is beneficial and to what extent?

3.2 Surface Flowfield Visualization: A Qualitative Study

The surface flow field was then visualized to further characterize the nature of the separation region on the model. In general, the surface flow streamlines are skin friction lines as they are formed under the influence of wall shear stresses rather than pressure gradients. However, this is not true for reverse flow regions where the surface shear stress is very small and the motion is a result of both shear stress and pressure gradient. As such, the lines of separation indicated by the flow pattern are normally ahead of the actual separation location[25]. The surface streamline pattern for flow without control is shown in Fig. 4a. Also sketched on Fig. 4a, are the streamlines indicating the flow direction. These streamlines have been drawn based on the visual observations during the experiment.

The horizontal streamlines in the upstream, left half, of Fig. 4a indicate that the flow field is fairly uniform and relatively two-dimensional in this region. However, three-dimensional effects can be observed immediately downstream of the ramp leading edge. The ‘secondary flow’ near the ramp edges also (see Fig. 4a) appears just downstream of the location where the ramp begins. This secondary flow may in part be due to corner vortices generated at the edges of the model, however its exact nature and its effect, if any, on flow separation is not clear at this point.

The reverse or separated flow region is also indicated in Fig. 4a. The surface streamlines emanating from the front stagnation point (S1) form a separation bubble, which ultimately spirals around two focal points F1 and F2. These focal points are also the point of local pressure minima. The streamlines then reattach at S2. In essence, the surface flow pattern shows a ‘trapped’ separation bubble, generated due to the ramp. The effect of flow control on the surface flow pattern is shown in Fig. 4b. As seen in this surface flow trace, no regions of reverse velocity are visible. The flow pattern, however, is not completely two-dimensional and three-dimensional features, such as diverging streamlines, can be noticed. As discussed later, it is anticipated that one of the mechanism at work in the present control technique is the introduction of streamwise vorticity by the microjets. As such, one may argue that some of the features in Fig. 4b are similar to footprints of streamwise vortices. However, at present the exact nature of these features is not clear. What is clear is the fact that the microjets eliminate the large 3D separation bubble seen in

Fig. 4a. In the following sections, we examine the flowfield in further detail using the velocity field measurements to better quantify the effect of microjets on the separated flows.

To verify the shape of the separation bubble above the surface, PIV measurements were subsequently obtained along the centerline plane and at two planes away from the centerline, as described in §2. Only velocity-field data for the 'Centerline' plane (see Fig. 2b) has been presented here for the sake of brevity.

3.3 Particle Image Velocimetry

The flow field above the surface was quantitatively studied using the two-dimensional (2-D) Particle Image Velocimetry (PIV) technique, which provides two components of the velocity in a given plane. The test section was seeded with smoke particles, approximately 5μm in diameter, using a Rosco fog generator. A New Wave™ Nd-YAG pulsed laser with a repetition rate of 15Hz was used to illuminate the particles introduced into the flow field. Each PIV image pair was then acquired using a Kodak ES 1.0 high-resolution CCD camera capable of recording 10-bit digital image pairs in separate frames at a rate of 15-image pairs/second. Further details of this PIV technique can be found in Lourenco[26] et al. One of the main advantages of this PIV technique is a novel processing scheme with high spatial resolution that uses image matching to extract the particle displacements, hence the velocities, from particle image pairs[27].

3.3.1 Baseline Case:

A typical processed instantaneous velocity vector field for the no control case, obtained using the PIV technique, has been shown in Fig. 5a. Smoke was introduced from the surface ports in the upstream section of the model and the entrained particles were visualized using a thin laser sheet generated using an Nd-YAG laser. A significant reverse flow region is clearly evident. A discussion of the flowfield with microjets activated at 25 psig, shown in Fig. 5b is delayed until the effect of control is discussed later in the paper. For a better understanding of the separation region and the effect of microjet control, mean flow properties are presented next.

Fig. 6a show the streamwise component U, of the mean velocity field in the centerline plane, corresponding to a freestream velocity of 40m/s. Note that in these and all subsequent PIV data included in this paper, the ramp model is on the top of the plot; the freestream flow is from left to right and the microjets issue from the top. The inset in Fig. 6a shows the ramp geometry and the region where the PIV data was obtained. In these plots, all the distances are non-dimensionalized with respect to the ramp height. The y-axis represents the vertical distance from the base of the ramp and the x-axis is the streamwise distance from the ramp leading edge (Refer to Fig. 2a for the origin of the coordinate frame).

A closer look at the plot shows that as one proceeds downstream in the vicinity of the surface, there is a rapid deceleration in the fluid velocity, which eventually leads to a region of reverse flow. This reverse flow zone corresponds to the dark blue velocity contours (Fig. 6a) and starts around $x/H = 1.6$ and approximately ends around $x/H = 2.2$ (corresponding to a physical length of approximately 2 inches). A small sub-region of this flow field, roughly indicated by the box in Fig. 6a, has been magnified in Fig. 6b, which shows the velocity vectors. The presence of reverse flow, close to the ramp surface, is clearly visible in this plot, indicating that the flow has separated locally resulting in a separation bubble with recirculating flow. Although not included in this paper for the sake of brevity, the presence of reverse flow was further confirmed by examining the vertical component of the velocity (perpendicular to freestream). Contour plots of this velocity component clearly reveal the presence of low magnitude velocity fluid moving away from the boundary in the same region where reverse flow field is seen in the streamwise velocity components. As noted by other researchers[15], it was also observed that increasing the freestream velocity causes the flow to separate further upstream, while the flow attachment location does not change appreciably, leading to a larger separation region. Though these results are not included here, freestream velocities up to 65 m/s were examined, resulting in much larger separation zones than the 40 m/s case discussed in this paper. These larger separated flows were subsequently controlled using microjets.

As noted earlier in the discussion of the surface flow traces, this separation appears to be three-dimensional in nature. Hence, ideally, one would like to obtain velocity measurements in planes perpendicular to the freestream flow, i.e. in the Y-Z plane (see Fig. 2b); such measurements are planned in future experiments. At present, PIV measurements were obtained at three off-centerline axial planes to provide some insight into the three-dimensional effects. Although not shown here, a comparison to the centerline velocity field (Fig. 6a) reveals that as one moves away from the centerline plane, the size of the bubble at grows appreciably larger (at the 0.4W plane) and then reduces as one approach the sides of the ramp. This result is consistent with our earlier observation based on the surface flow pattern.

3.3.2 Effect of Microjet Control

The visual effect of the microjets can be seen from the instantaneous velocity vector field in Fig. 5b, obtained using PIV. The image was obtained with the 3rd array of microjets, MJ3, operating at 25psig. A comparison with Fig. 5a, clearly illustrates that not only has the reverse velocity zone been eliminated, but, there has also been a significant momentum addition along the surface. To study this effect of microjets, the influence of various parameters on separation control was examined, as described next.

The first parameter considered was the freestream velocity. Fig. 7a presents the streamwise velocity data for the centerline plane at 40m/s, where the 3rd array of microjets is operating at 25psig. A comparison of Fig. 7a with Fig. 6a shows that the activation of microjets completely eliminates the reverse flow region; very similar effects were also observed for the 50m/s case, where the separated flowfield was 15-20 % larger. It was also noticed that at 40m/s, the velocity measured with control near the surface was somewhat higher than for the 50m/s case. This suggests that the ratio of the microjet momentum relative to the freestream momentum may be an important parameter. This effect of the momentum flux ratio is of course well known and has been discussed by numerous other investigators[20].

To quantify the efficacy of microjet control in terms of the mass and momentum flux supplied by the microjets, the mass flux coefficient, M^*, and the steady momentum coefficient, C_μ were defined as follows:

M^*= (Mass flux of the microjets) / (Mass deficit based on δ)

where, δ is the boundary layer thickness at the ramp leading edge.

The mass flow rate, m_{in}, through the supersonic microjets can be conservatively estimated by assuming choked flow through the micro-nozzles. The mass coefficient is then given as:

$$M^* = \frac{m_{in}}{\rho_\infty U_\infty y \delta}$$

where, ρ_∞ is the freestream density, U_∞ is the freestream velocity, and y is the span of the ramp.

The momentum flux ratio is given by the conventional definition of the steady momentum coefficient[20] and is given as

$$C_\mu = \frac{N m_{in} U_j}{\frac{1}{2} \rho_\infty U_\infty^2 y \delta}$$

where N is the number of microjets, and U_j is the jet velocity.

Thus, C_μ is the ratio of the magnitude of the total momentum injected into the flow relative to the freestream dynamic pressure multiplied by an appropriate area – chosen as δy in the present case. These values of C_μ and M^* for various microjet operating pressure have been plotted in Fig. 8. As expected, C_μ and M^* are related such that small increments in M^* yield progressively larger C_μs, thus accounting for the effectiveness of microjets with relatively little mass flow injection. Measurements show that increasing the microjet operation pressures, i.e. increasing the C_μ results in higher velocities closer to the ramp surface, indicating the presence of higher momentum in the near-wall region. The reason behind this behavior may be due to one or more of the following; as C_μ increases a) more momentum is directly injected into the boundary layer, b) strong streamwise vortices[22] are generated which enhance mixing with the outer, high momentum fluid and or c) The microjet jet momentum and penetration depth[28, 29] increases, enhancing the transfer of momentum from the freestream fluid to boundary layer fluid.

A magnified view of a selected region for the 40m/s case (Fig. 7a) is shown in Fig. 7b, in the form of a velocity vector plot. A comparison with the corresponding plot, Fig. 6b, shows that with the activation of microjets, velocity vectors in the zone previously corresponding to reverse flow now possess significant momentum in the forward direction. At 25 psig, the mass flux supplied by the microjets is approximately 1.7 % of the mass flux across the ramp, based on the boundary layer thickness, i.e. $M^* = 0.017$. This pressure corresponds to a C_μ of 0.397 or 39.7%, which amounts to a C_μ of 6.3e-03/jet, which is much higher than the 2e-03/jet value quoted by Amitay[18].

In general, any separation control input must be applied at or close to the separation point. To investigate the effect of the actuator location, experiments were conducted with microjets at different axial locations along the ramp. The microjets were successful in eliminating the reverse flow region regardless of their location. However, upon comparing the effect of MJ1 with the results shown in Fig. 7a, for the 3rd array of microjets (MJ3), it appears that, although both microjet arrays were able to eliminate separation, higher velocities closer to the surface were obtained with the activation of MJ3. In addition, the reverse flow region was eliminated with a lower momentum flux input using MJ3 compared to MJ1, indicating that, as expected, choosing an appropriate location to apply flow control is an important parameter for optimal flow control.

Whether the microjets eliminate the entire three-dimensional separation region was also examined using the PIV results acquired at the Off-Centerline locations. Although separation was completely eliminated, it was noticed that the effect of control was not as pronounced as in the centerline plane. For example, the magnitude of the U component of the velocity, near the ramp surface was somewhat less than the velocities measured along the centerline. The reasons for this are attributed to the three dimensional nature of the separation bubble and perhaps also due to the presence of secondary corner flow as discussed in § 3.2. Although the details of the effect of microjets at off-centerline locations are not completely understood at present, there is no doubt that overall, they have a beneficial effect in that the microjets eliminate or significantly reduce the size of the separation region. An examination of the three-dimensional effects is the main focus of ongoing research at our laboratory.

4. Microjets: A Closer look at Effect of Control and Flow Mechanisms

In order to determine whether the significant increase in the momentum near the ramp surface is simply due to the direct injection of momentum by the microjets, we define a parameter referred to as the 'momentum gain ratio', ***MGR***. It is the ratio of the increase in momentum due to microjet control relative to the momentum injected by the microjets. Hence, MGR is given as:

$$MGR = \frac{momentum_{With\ Control} - momentum_{No\ Control}}{momentum_{microjets}} = \frac{\int(\rho U dA)_{With\ Control} - \int(\rho U dA)_{No\ Control}}{N\dot{m}_{in}U_j}$$

The momentum flux with and without control was calculated at axial locations by numerically integrating the velocity field data. A comparison of the momentum gain achieved with the application of different microjets at various operating pressures is listed in Table 1 and a corresponding plot is shown in Fig. 9. Both the tabulated results and the plot clearly show that for the same C_μ values the momentum gain achieved with MJ3 is significantly more than that achieved with MJ1. In particular, at 25psig, the momentum gain with MJ1 is 7.8, while the momentum gain achieved with MJ3 is 30. This reaffirms the notion that the location of the actuators relative to the separation location plays a very important role in the efficacy of control. Furthermore, it suggests that closer one is to the separation location; more effective control can be achieved.

This high momentum gain ratio clearly indicates that some other mechanism(s), distinct from direct injection of momentum plays an important role in this control approach. As mentioned earlier, one of the physical mechanisms we expect to be of significance is the generation of streamwise vorticity by the supersonic microjets[22, 30]. This streamwise vorticity is expected to enhance the entrainment of the freestream fluid into the boundary layer. In addition, it may also promote mixing between the low momentum portions of the boundary layer, very close to the surface, with the higher momentum fluid away from the wall, thus preventing or delaying separation.

To further explore and understand the effect of the microjets, we sought to delineate the effects of flow control on the momentum gain (MGR) into two regions as follows. We first identify a region where the near-wall fluid 'directly' encounters the microjets and define its extent as the maximum penetration depth of the microjets. Hence, this defines the zone in which the microjets may influence the local flow directly. The second zone is the remainder of the boundary layer flow outside the area of direct influence. In this second zone, the gain in momentum due to flow control may be more strongly influenced by other mechanisms, such as the generation of streamwise vorticity, physical mechanisms that we collectively refer to as the 'secondary effects' of the microjets. As documented by others[22, 31], the penetration depth of jets in cross-flow is mainly a function of the momentum ratio. Although there are a number of primarily empirical correlations available in literature for estimating the penetration of jets in cross-flow, for the present analysis, the maximum jet penetration, Y_{max} of a single jet into a duct with a cross-flow was evaluated using Norster's equation[28].

$$\frac{Y_{\max}}{d_j} = 1.15 \times \left(\frac{\rho_j U_j^2}{\rho_\infty U_\infty^2} \right)^{0.5} \times \sin(\delta_j)$$

where $\boldsymbol{\rho_j}$ is the jet density, $\boldsymbol{d_j}$ is the jet diameter and $\boldsymbol{\delta_j}$ is the microjet blowing angle at the *vena contracta*.

Using the above correlation, the penetration of the microjets was determined to be approximately 0.2″, almost 1/4th of the boundary layer thickness. This leads to the definition of the region of direct influence as that below this 'quarter' boundary layer plane, $\boldsymbol{\delta_{0.25}}$. Outside $\delta_{0.25}$, one would expect the gain in momentum to be due to the secondary effects, as discussed above. Using these definitions, the momentum again ratio for MJ3 operating at 25psig is evaluated at various axial locations for both the direct and secondary effects and the results are shown in Fig. 10. The plot shows that downstream of the microjet injection location, the 'direct effect' initially starts to grow rapidly. This initial rapid growth of the directly effected zone occurs in the vicinity of the microjet injection location, a region generally identified as where the initial evolution – penetration into and turning due to the freestream flow – occurs[32, 33]. Further downstream, the momentum gain due to the direct effects appears to saturate and even decline. However, the contribution of the secondary effects continues to grow downstream of the injection location and plays a proportionally larger role as one move downstream. This suggests that the secondary effects - which we suspect to be due to the generation of streamwise vorticity – continue to energize the boundary layer flow by entraining high momentum fluid from the freestream.

We recognize that there are many ways in which one can examine the results obtained in our study to better elucidate the flow physics behind this control technique; the preceding analysis and discussion is a one simple, phenomenological-based, attempt to do so. This is an issue that we are continuing to study further and in more detail and hope to gain a better understanding through additional experiments and analysis. However, it is clear at this point that the present control technique is not effective simply due to the direct injection of momentum into the boundary layer of fluid.

Next, we briefly examine the effect of microjets on the flow unsteadiness. Fig. 11a and 11b present the fluctuating component of the streamwise velocity, U_{rms} for the uncontrolled and the controlled cases, respectively. As before, these results correspond to a freestream velocity of 40m/s where the 3rd array of microjets (MJ3) was activated at 25psig for the controlled case. In these contour plots, U_{rms} has been non-dimensionalized with the freestream velocity. A comparison of Fig. 11a with Fig. 11b, illustrates that the velocity fluctuations associated with the flow have been dramatically reduced, by as much as 50% or more. In fact, most of the regions associated with high fluctuations have disappeared. Not only have the velocity fluctuations have been reduced in magnitude, but also the regions in which these fluctuations occur have become much smaller. Although not shown here, a comparison of turbulence kinetic energy associated with the uncontrolled and controlled cases was also made[34]. It was observed that level of turbulence associated with the flow was also reduced by almost 50%; similar effects were observed at higher freestream velocities.

To summarize, although the physical mechanisms behind microjet control still need to be explored further, based on the use of microjets in other applications[21, 23, 30] and on our present results, it appears that the streamwise vorticity due to the microjets may play a primary role in this control approach. The generation of streamwise vorticity can be due to a number of mechanisms. First, the microjets may behave as fluidic ‘tabs’ much like the micro-v.g.’s used in earlier work[14,15,19]. Second, the vorticity in the microjets is redirected in the streamwise direction by the mean flow, and finally the microjets may also redirect the spanwise vorticity in the base flow in the streamwise direction by vorticity ‘tilting’. These mechanisms may be similar to those discussed by Alvi et al.[30] in the context of impinging jet control using microjets.

5. The New Test Model

Within the constraints of our first-generation ramp model, we explored the effect of some of the above parameters on the separated flow and the efficacy of microjet control. The first parameter is nature of pressure gradient itself, which in our case is of the "Stratford" kind. The adverse nature of the pressure gradient generated by the ramp caused the flow to separate and subsequently reattach downstream, enclosing a separation bubble. As expected, the Reynolds number also affected the separation location and size. It was observed that an increase in the freestream velocity from 40m/s to 50m/s caused the separation region to grow by almost 15 % and also the separation location moved upstream. The third parameter examined is the location of microjets with respect to separation location, x/L. The results indicate that closer the microjets are to the separation location, more effective they are in controlling flow separation. The final parameter explored was the relative (to the freestream) magnitude of the momentum supplied by the microjets which is quantified as C_μ. As C_μ is increased, the flow near the surface became 'fuller', marked by a noticeable increase in velocity near the surface. It was observed that with very low amount of mass flux (less than 1.5%), corresponding to a C_μ as high as 29.1%, we were able to very effectively control flow separation.

With the lessons learnt from our initial study, a more flexible geometry both in the terms of the severity of separation and the microjet control parameters was needed.

6. Microjet Control Further Explored Using the New Model

Some parameters that are expected to have a significant effect on the separation location, size and the control mechanism are as follows:

- Nature of pressure gradient, dp/dx (i.e. ramp geometry)
- Reynolds number, Re
- Location of microjets w.r.t. separation location
- The relative momentum supplied, by the microjets, referred to as the momentum coefficient, C_μ.
- Angle at which momentum is supplied to the boundary layer
- Angle of attack of the ramp, θ.
- Spacing between the microjets.

To explore these parameters in a more detailed way and consecutively, to obtain a better understanding of the physical mechanisms responsible for the effectiveness of microjet control, a new model was designed and fabricated. The new model is highly flexible, allowing us to change the base flow as well as the control parameters. For example, the ramp can be rotated about a pivot point giving us the flexibility to change the adverse pressure gradient experienced by the flow, thereby controlling the nature – size and location – of the separated flow.

This model has 29 static pressure taps along the centerline and more than 60 pressure taps along the transverse direction at tactical locations. A picture of this model, fabricated out of Aluminum, is shown in Fig. 12a. It also has 7 arrays of supersonic microjets incorporated on a separate insert shown in Fig. 12b. The microjets are 400μm in diameter with spacing of 5mm (could be changed) and are located strategically around the separation location, keeping in mind the change in separation location with change in angle of attack. This microjet insert has slots for microjet modules (Fig. 12d). These modules are capable of supplying momentum at various angles and are interchangeable. A magnified view of the module revealing microjets has also been shown in Fig. 12d. The locations of these microjets and the modular insert are also shown in Fig. 13a and Fig. 13b. These flexibilities in the ramp model allowed us to study the parametrical effects on separation location in much detail.

With the knowledge gained about the flow-field from our initial set-up, we concentrated mostly on the quantitative analysis of the flow field. Quantitative velocity field data was obtained using 2D-PIV along the centerline plane. The location of these PIV measurements is shown in Fig. 13a and 13b.

6.1 2D-PIV: Microjets Revisited

6.1.1 Baseline Case

A representative of the ensemble averaged velocity field for freestream velocity of 40m/s has been shown in Fig. 14 where the ramp is at an angle of 5° (see Fig. 13b) and flow is from left to right. In these plots, length scales are non-dimensionalized with respect to ramp height, H. (Note that increasing the ramp angle corresponds to increasing the adverse pressure gradient on the ramp surface). A closer look at Fig. 14a reveals that as one proceeds downstream in the vicinity of the surface, there is a rapid deceleration in the fluid velocity, which eventually leads to a region of reverse flow. This reverse flow zone which corresponds to dark blue velocity contours, starting at around X/H=1.7 and extending till X/H=3.1, where H = 2.25″, indicates that flow has separated locally and a separation bubble with recirculating flow is visibly present. In physical dimensions, the separation region for this case is ~3.2″, which is considerably larger to the case where the ramp is at lower angles, e.g. for 0° case, the recirculation bubble is only ~1.9″. This of course is expected, since higher ramp angles results in more adverse pressure gradients hence larger separation regions. A sample case of the velocity field at 65m/s, with a ramp angle of 5°, is also shown in Fig. 15. A comparison to the 40 m/s case of Fig. 14, shows that the recirculation bubble is significantly larger, both in extent and magnitude. The contour levels have been modified to adjust the velocity changes. Although not shown here, similar results can be observed from the vertical velocity component also where low magnitude velocity moving away from the boundary can be observed in the same region where reverse flow field is seen in the streamwise velocity plots.

To summarize, the adverse pressure gradient generated due to ramp geometry leads to local separation of the incoming boundary layer, where the size of the bubble increases with the freestream velocity and ramp angle (adverse pressure gradient).

6.1.2 Effect of Microjet Control

When microjets were turned on at suitable locations, it was observed that, the reverse flow or the separated flow region is eliminated, with very low mass flux. This result can be verified by the velocity contour plot shown in Fig. 14b where the microjet array at *mj4*, at an angle of 90° relative to the local surface, has been activated at a stagnation pressure of 10psig. This effect of microjets was observed for all the conditions where the separated flow was present for the baseline case. A comparison with Fig. 14a (No control) indicates that with the activation of microjets not only was the reverse flow eliminated but the momentum near the surface is increased significantly. This effect of microjet control and the optimization procedure, i.e. identifying parameters to formulate a control strategy which has a maximal impact with minimal effort is presently being explored in detail. As a first step, we have presented the effect of microjet location later on in this report. Similar effect of control was observed at the highest velocity examined (65 m/s), where the extent and the magnitude of the separation region were much greater. This can be confirmed from Fig. 15b, where microjet *mj5* at an angle of 90° to the ramp surface has been activated at 25psig and separation is completely eliminated.

7.1.2.1 Effect of Microjet Location

The location of the actuation has been found to be critical by numerous investigators[19]. It stands to reason and is generally believed that actuation closer to the separation location would produce the most beneficial results. From our velocity field measurements, the separation location for the given flow conditions was known. Accordingly, the flowfield was examined for a number of cases where the microjet actuators were placed at varying distances, both upstream and downstream, relative to the separation location. As discussed subsequently, in some detail, the velocity field data reveals that in general the microjets are most effective when activated upstream of the separation location. There appears to be a range of locations upstream of separation, where their effect is optimal; once outside this range, either very close or too far upstream, the effect of control diminishes. Similarly, locating the actuators downstream of the separation is also non-optimal. However, for all the actuator locations examined to date, separation control could be achieved when the microjets were operated at the appropriate pressure. This required pressure increases as one moves outside the optimal actuator placement zone.

To facilitate our discussion, Table 2 provides the approximate locations for the separation, and the actuators. A representative example of the velocity profiles for the 40 m/s case at a ramp angle of 5° is presented in Fig. 16, where U/U_{inf} is shown as a function of the vertical distance from the surface (Z/H) at a streamwise location of X/H=2.3. The location at which this data was extracted from the velocity field is shown as a dashed vertical white line on Fig. 15. For the controlled cases, the microjet angle relative to the surface is 68° and the microjet stagnation pressure is 10psig. As evident in Fig. 16a, different locations have a different effect on the velocity profile. Keeping in mind that for this case, the flow separates roughly at X/H~1.7, the activation of *mj2*, which is significantly far upstream (at X/H ~ 0.7), at 10 psig does not lead to complete attachment and very small reverse velocities can still be seen in the plot (*mj2*: green curve). In contrast, the flow is completely attached and the velocity profiles become much ‘full’ with the activation of *mj5* (orange curve), which is located at X/H~ 1.3, i.e. much close but upstream of separation. Along the same lines, when *mj7* (@ X/H ~ 1.9, located downstream of the separation location, is activated the velocity profile deteriorates slightly relative to mj5, although the difference is minimal.

With proper use of other control variables, this mass flow requirement is expected to go down further. Question is “how much lower?” OR “What should be the criterion for control?” Should the criterion just be that the flow is incipiently attached everywhere or should the increase in the momentum in the near-wall region of the boundary layer, i.e. the fullness of the boundary layer profile, be also considered? The answer to this question will likely come from a detailed cost function analysis, which is beyond the scope of this paper. What the present results show however is that the microjet pressure needed for the flow to be incipiently attached is ~5psig. When extrapolated to a theoretical inlet duct, e.g. a 30% boundary layer ingesting duct – a nominal value used for BWB inlet, this results in a mass flow requirement that is well below the maximum permissible bleed flow values as quoted by engine manufacturers. This suggests that engine bleed flow may be used to supply the gas for the microjet actuators.

7. Concluding remarks and Future work

To summarize, our results till date based on PIV data show the dramatic effect of microjets in controlling flow separation, at least in the present test geometry. Our results indicate that the effect of microjets varies with the amount of momentum supplied via the microjets (which is proportional to microjet pressure) and also with their location and angle at which momentum is injected. These controlling parameters are coupled together, but yet by changing any variable, with sufficient pressure, the separated flow can be attached.

The mechanism, as anticipated and as discussed before, is that these microjets serve the dual purpose of energizing the low momentum boundary layer flow and also act as "Fluidic Vortex Generators[21]" to prevent or delay separation. These vortices promote the mixing of lower momentum boundary layer fluid with outer higher momentum fluid and this enhanced mixing helps to control or delay the separation. The most significant advantage of using these microjets is that they can be turned on or off, as and when desired, thereby eliminating the associated penalty of reduced drag as with the conventional vortex generators. In addition, they are "very low mass-high momentum" devices, which make them all the more attractive from a practical point of view.

In the next stage of the research, we plan to study the three-dimensional nature of this flow and the effect of the flow and control parameters in much more detail. Specifically, we plan on obtaining 3D-PIV measurements to examine and identify the details of the physical mechanisms behind microjet flow control. We also plan to use unsteady pressure transducers as sensing devices for the separated flow (indicating location and the magnitude of separation) and correspondingly control the flow using a closed loop control strategy. Through a much better understanding of these properties, we hope to devise a more optimal microjet-based control scheme.

8. References

1. MacMartin, D.G., Verma A., Murray R.M., Paduano J.D., "Active Control of Integrated Inlet/ Compression systems" FEDSM2001-18275, June 2001.
2. Mayer, D.W., Anderson, B.H., Johnson T.A., "3D Subsonic Diffuser Design and Analysis", AIAA Paper 98-3418.
3. Wellborn, S. R., Reichert, B.A., Okiishi, T.H., "Study of Compressible Flow in a Diffusing S-Duct", *Journal of Propulsion and Power*, Vol. 10, No. 5, Sept-Oct 1994, pp. 668-675.
4. Liebeck, R.H., "Design of Blended Wing Body Subsonic Transport", *Journal of Aircraft*, Vol. 41, No. 1, January-February 2004.
5. Rabe, D., Boles, A. and Russler, P. "Influence of Inlet Distortion on Transonic Compressor Blade Loading", AIAA Paper 95-2461.
6. Wygnanski, Seifert A., "Delay of Airfoil Stall by Periodic Excitation" *AIAA J Aircraft* 1996; Vol. 33(4):691–8.
7. Chang, P.K., "Control of Flow Separation", Hemisphere Publishing Corporation and McGraw Hill, New York, USA, 1970, pp. 154-177.
8. Gad-el-Hak M, Bushnell D.M., "Separation Control: A Review", *Journal of Fluids Engg.*, 1991; 113:5-30.
9. Schlichting H., "Aerodynamische Probleme des Höchstauftriebes" Z. Flugwiss. Bd. 13, 1-14.
10. Thomas F., "Untersuchungen über die Erhöhung des Auftriebes von Tragflügeln mittels Grenzschichtbeeinflussung durch Ausblasen" Z. Flugwiss., Bd. 10, 46-65.
11. Mokhtarian F., Modi V.J., "Fluid Dynamics of Airfoils with Moving Surface Boundary Layer Control," *Journal of Aircraft*, 1988, Vol. 25, pp.163-169.
12. Prandtl L. "Proceedings of Third International Mathematical Congress", Heidelberg, 1904, p. 484-91.
13. Betz A. "History of Boundary Layer Control", Germany. In: Lachmann GV, editor. Boundary Layer and Flow Control: Its Principles and Applications, Vol.1, New York: Pergamon Press, 1961. pp. 1-20.
14. Storms B. L, Ross JC. "Experimental Study of Lift-Enhancing Tabs on a Two-Element Airfoil." *AIAA J Aircraft* 1995; Vol. 32: 1072-8
15. Lin, John C. "Review of Research on Low Profile Vortex Generators to control Boundary Layer Separation", *Progress in Aerospace Sciences* Vol. 38(2002), p. 389-420.

16. Zaman K.B.M.Q., Bar Sever A, Mangalam S.M., “Effect of Acoustic Excitation on the flow over a Low-Re Airfoil”, *Journal of Fluid Mechanics*, 1987,182:127-48.
17. Ahuja K.K., Whipkey R.R., Jones G.S., “Control of Turbulent Boundary Layer by Sound”, AIAA Paper 83-0726, 1983.
18. Amitay M., Pitt D., Glezer A. “Separation control in duct flows”, *Journal of Aircraft* Vol. 39, No. 4, July – August 2002.
19. Jenkins, L.N., Gorton, S.A., Anders S.G., “Flow Control Device Evaluation for an Internal Flow with an Adverse Pressure Gradient” AIAA Paper 2002-0266.
20. Greenblatt David, Wygnanski, I.J., “The Control of Flow Separation by Periodic Excitation”, *Progress in Aerospace Sciences* Vol. 36(2000), p. 487-545.
21. Alvi, F. S., Elavarsan R., Shih, C., Garg G., and Krothapalli, A., “Control of Supersonic Impinging Jet Flows using Microjets,” *AIAA Journal*, 2003 Vol. 41(7), p. 1347-1355.
22. Johnston J.P., Nishi M., “Vortex Generator Jets- Means for Flow Separation Control”, *AIAA Journal*, 1990 Vol. 28, No. 6, pp.989-994.
23. Lou H., Alvi F.S., Shih C., “A PIV study of Supersonic Impinging Jet”, AIAA Paper 2003-3263, 9th AIAA/CEAS Aeroacoustics Conference and Exhibit, May, Hilton Head, South Carolina.
24. Stratford, B.S., “The Prediction of Separation of Turbulent Boundary Layer”, *J. Fluid Mech.* 5, 1-16, 1959b.
25. Barberpoulos A.A, Garry K.P., “The Effect of Skewing on the Vorticity produced by an Air jet Vortex Generator”, *The Aeronautical Journal*, March 1998.
26. Lourenco, L.M., “True Resolution PIV: A Mesh Free Second Order accurate Algorithm” International Conference in application of lasers in Fluid mechanics, Lisbon, Portugal, July 2000
27. Lourenco, L.M., Krothapalli A., “Mesh Free Second Order Algorithm for PIV Processing”, Proceedings of the International conference on Optical technology and Image Processing in Fluid, Thermal and Combustion Flows, Yokohoma, Japan, Dec. 1998, pp. 24.
28. Norster E.R., “Jet penetration and mixing studies”. Unpublished work, College of Aeronautics, Cranfield. See Reference 33.
29. Lefebvre, A.H., “Gas turbine combustion” McGraw Hill, New York, 1983.
30. Alvi, F.S., “The role of Streamwise Vorticity in the Control of Impinging Jets”, FEDSM2003-45062.

31. Papamoschou D., Hubbard D.G., “Visual Observations of Supersonic Transverse Jets”, *Experiments in Fluids* Vol. 14(1993), pp. 468-471.
32. Marzouk, Y. M., Ghoniem, A.F. “Mechanism of Streamwise Vorticity Formation in a Transverse Jet”, AIAA Paper 2002-1063.
33. Marzouk, Y. M., Ghoniem, A.F. “Vorticity formulation for an actuated jet in crossflow”, AIAA Paper 2004-0096.
34. Kumar, V., Alvi, F.S. “Use of Supersonic Microjets for Active Separation Control in Diffusers”, AIAA Paper 2003-4160.

9. Students Supported

The following students were in part supported by this grant during their graduate studies:

1. K. Phalnikar – MS, 2001
2. V. Kumar - MS, 2003; presently pursuing a PhD (expected completion, Fall 2006)
3. C. Davy – MS, 2003
4. O. Egungwu - MS, 2004

10. Publications Resulting from Research Supported by this Grant

1. Kumar, V. and Alvi, F. S., “Use of High-Speed Microjets for Active Separation Control,” to appear in the *AIAA Journal* in early Spring 2005; accepted for publication in June 2005.
2. Kumar, V. and Alvi, F. S., “Active Control Of Flow Separation Using Supersonic Microjets,” ASME 2003 Fluids Engineering Meeting, July 6-10, 2003, Honolulu, Hawaii.
3. Kumar, V., Alvi, F.S. “Use of Supersonic Microjets for Active Separation Control in Diffusers”, AIAA Paper 2003-4160.
4. Davy, C., Alvi, F. S. and Naughton, J. W. “Surface Flow Measurements of Micro-Supersonic Impinging Jets,” AIAA Paper presented at the AIAA Ground Measurement Technology Conference, St. Louis, Missouri, 24 – 27, Jun 2002
5. Davy, C., Alvi, F. S and Naughton, J. W. “Flowfield and Surface Flow Measurements of Supersonic, Free and Impinging Microjets,” The 10th International Symposium on Flow Visualization, August 26-29, 2002, Kyoto, Japan.
6. Phalnikar, K. A., Alvi, F. S. and Shih, C. “Behavior of Free and Impinging Supersonic Microjets,” AIAA Paper 2001-3047, 31st AIAA Fluid Dynamics Conference & Exhibit 11-14 June 2001, Anaheim, CA.

List of Table Captions

Table 1: Momentum injected versus Momentum gain achieved for various microjet pressures.

Microjet activated	Microjet Pressure	C_μ (%)	Momentum Gain Ratio ***(MGR)***
MJ1	10	11.76	13.22
MJ1	15	19.58	9.53
MJ1	20	29.06	4.71
MJ1	25	39.71	7.44
MJ3	10	11.76	49.61
MJ3	15	19.58	40.38
MJ3	20	29.06	33.56
MJ3	25	39.71	28.78

Table 2: Ramp Configuration

Ramp Height (H)	*2.25″*	
	Approximate Locations (X/H)	
Microjets	*MJ2*	0.7
	MJ3	0.9
	MJ4	1.0
	MJ5	1.3
	MJ6	1.5
	MJ7	1.9
Separation begins	40 m/s	1.7
Reattachment	40 m/s	3.1

List of Figure Captions

Fig. 1- Ramp model, mounted in the wind tunnel

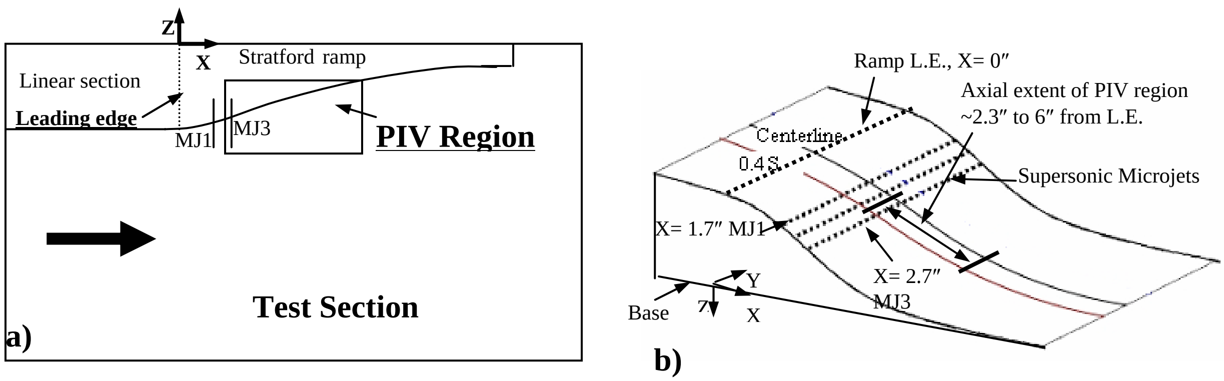

Fig. 2- a) Schematic of the test section

b) Detailed schematic of the ramp model

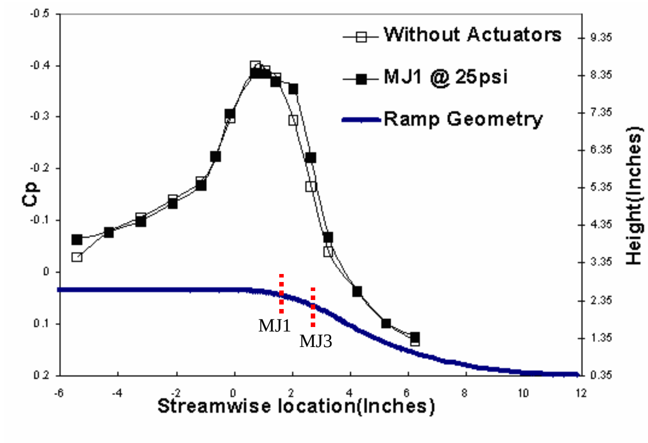

Fig. 3- C_p distribution along the centerline at 40m/s; with and without microjets.

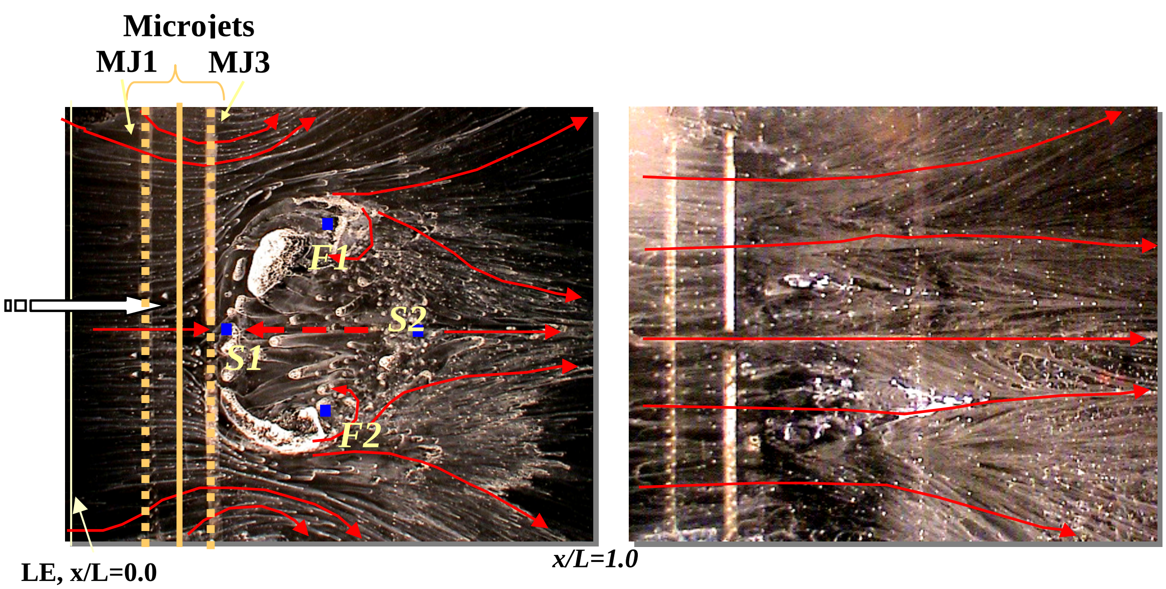

Fig. 4- Surface flow traces at 40m/s;

a) *No control* **b)** MJ3@25psig

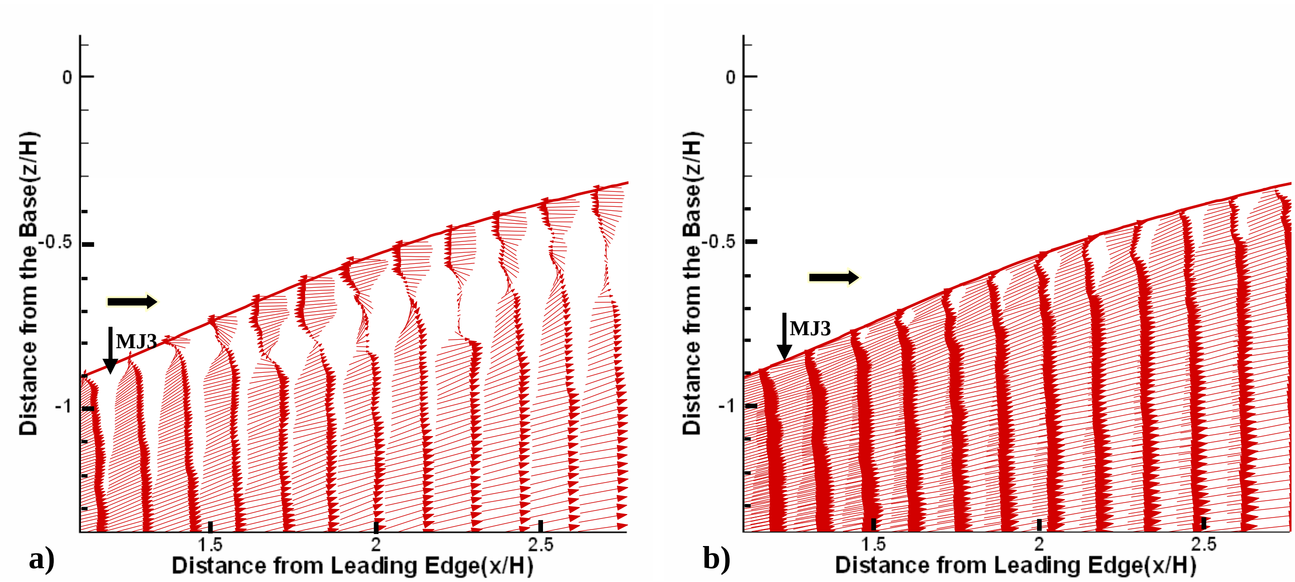

Fig. 5- a) Processed velocity vectors, *No Control* at 40m/s

b) Processed velocity vectors, *MJ3@25psig* at 40m/s

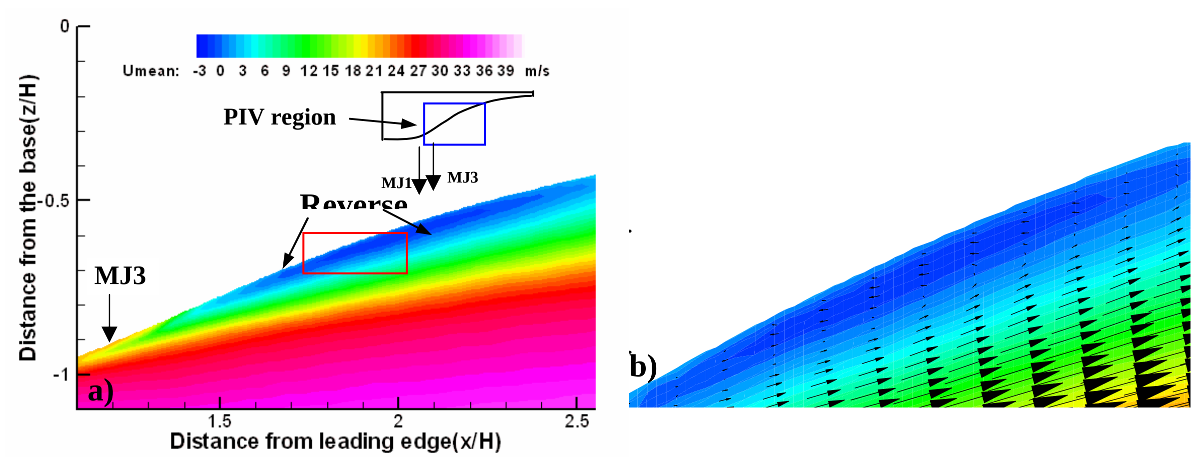

Fig. 6- Velocity field for 40m/s; *No Control.*

a) Streamwise velocity component, U **b)** Velocity vector for region indicated in (a)

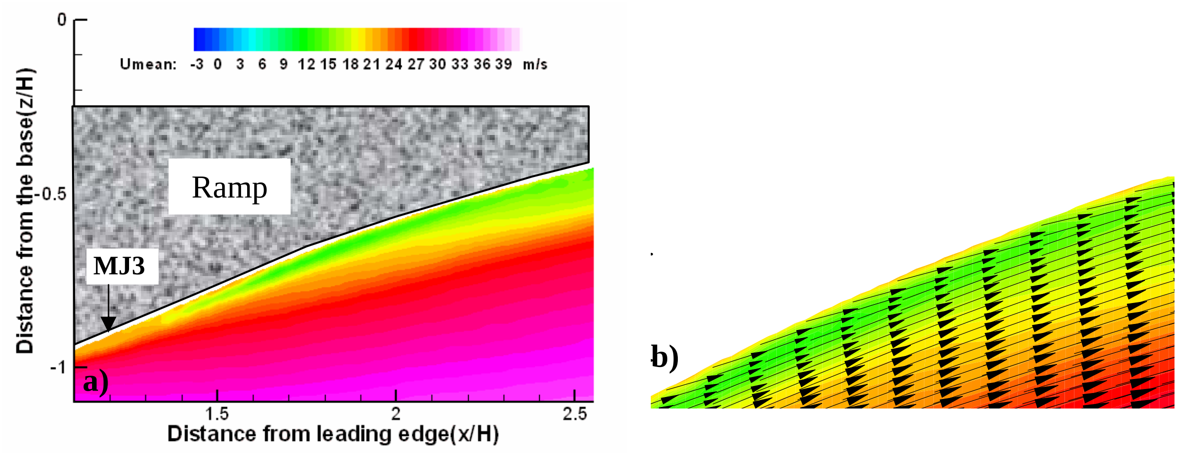

Fig. 7- Velocity field for 40m/s; *MJ3@25psig.*

a) Streamwise velocity component, U **b)** Velocity vector for region indicated in (a)

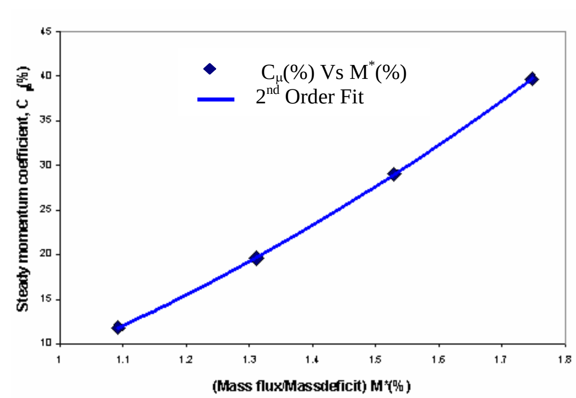

Fig. 8- Steady momentum coefficient, C_μ Vs. Mass flux coefficient, M^*

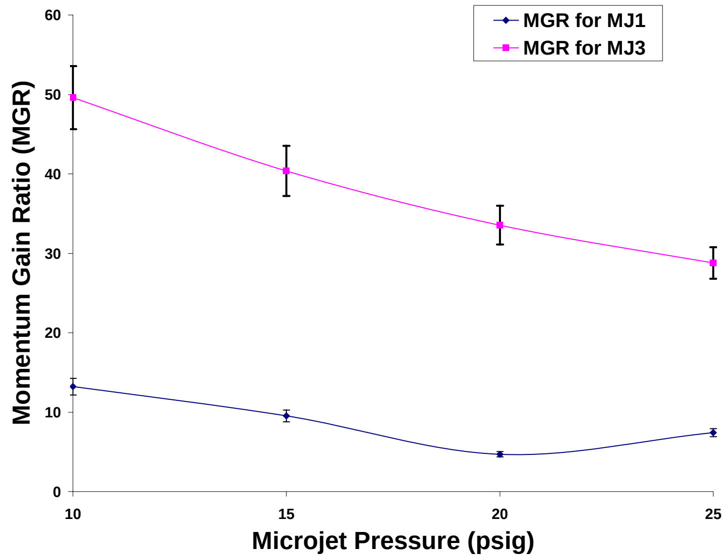

Fig. 9- Effect of Microjet location on MGR

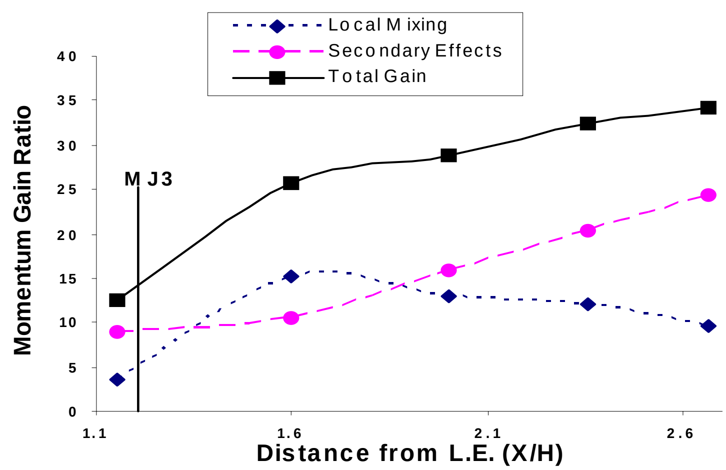

Fig. 10- A Comparative look at Microjet effects; MJ3@25psig

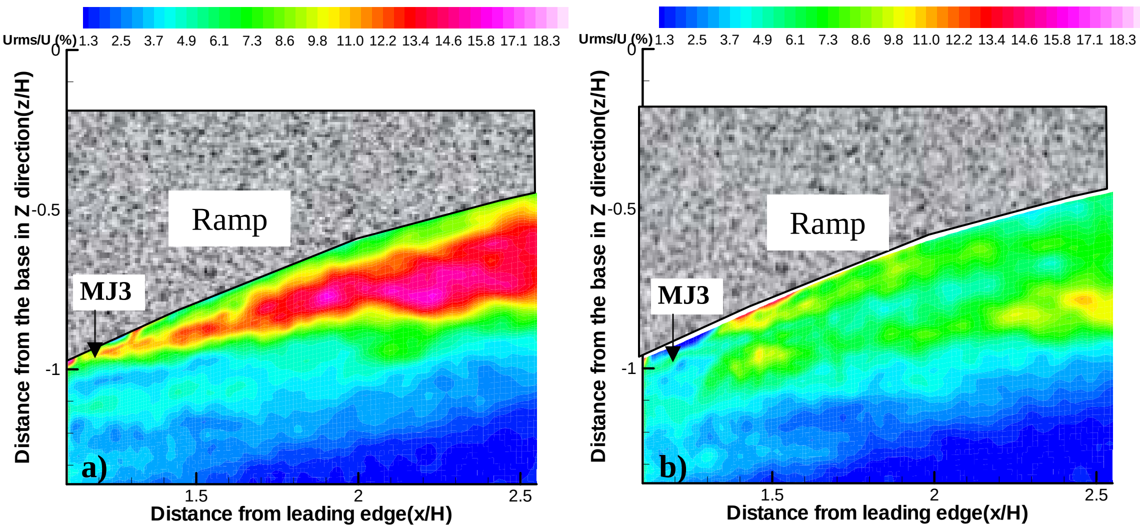

Fig. 11- Root mean square (U_{rms}) velocity;

a) *No Control* **b)** *MJ3@25psig*

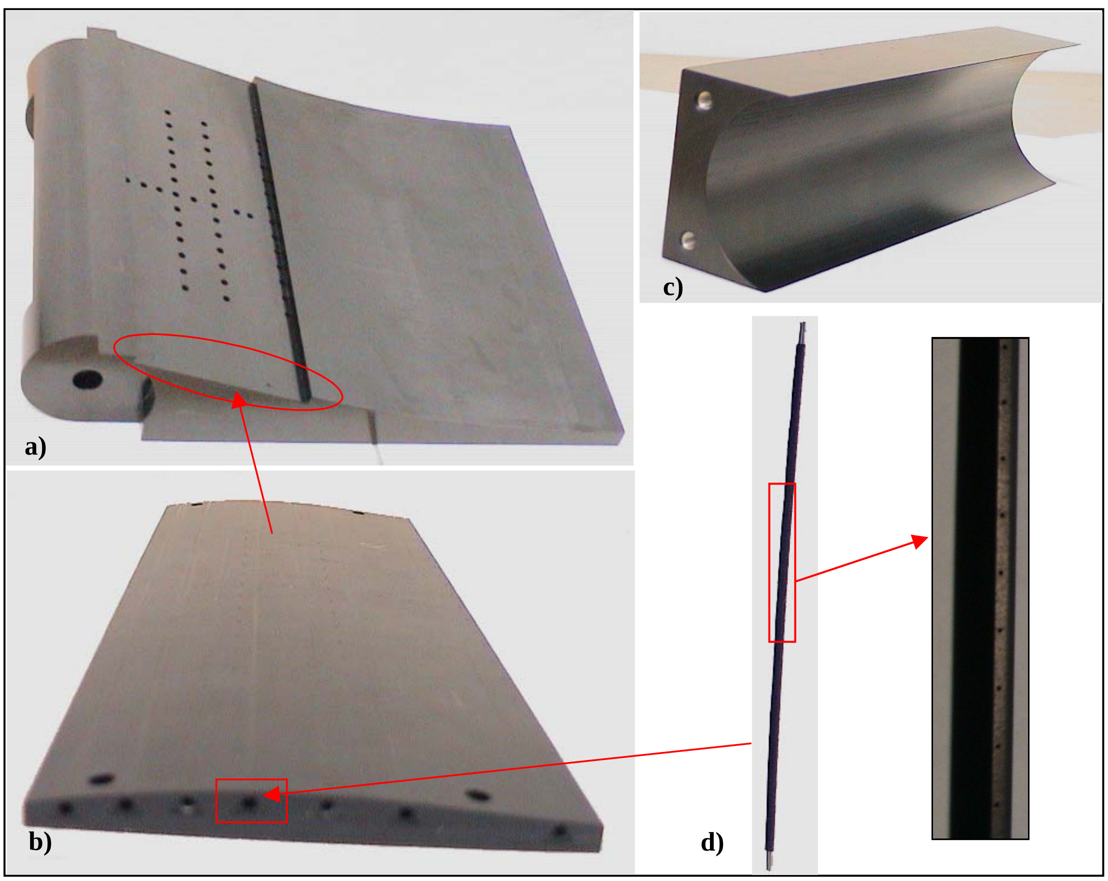

Fig. 12- a) New ramp model **b)** Microjet actuator insert which slides into the ramp model **c)** Hinge, to which the ramp attaches; allows for changes in ramp angle. **d)** Microjet array inserts which slide into the insert shown in b).

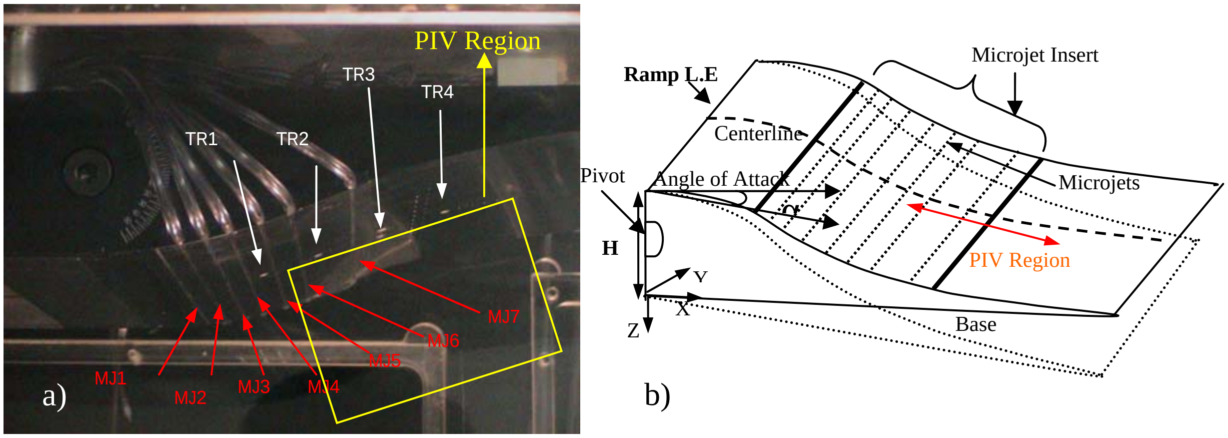

Fig. 13- a) Test model mounted in the test section

b) Schematic of the test model

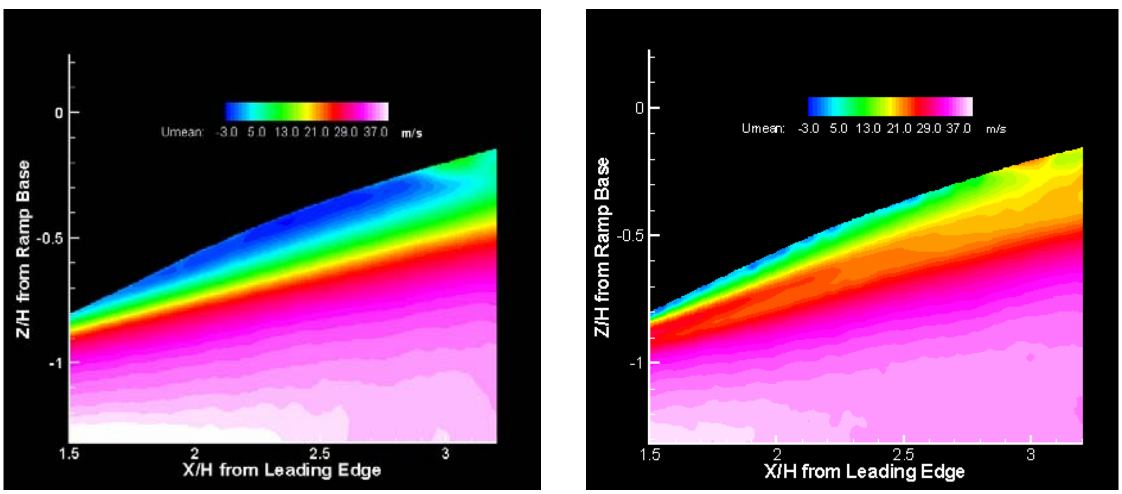

Fig. 14- a) Streamwise velocity data @40m/s: No Control

b) Streamwise velocity data @40m/s: MJ4; 90°; 10psig

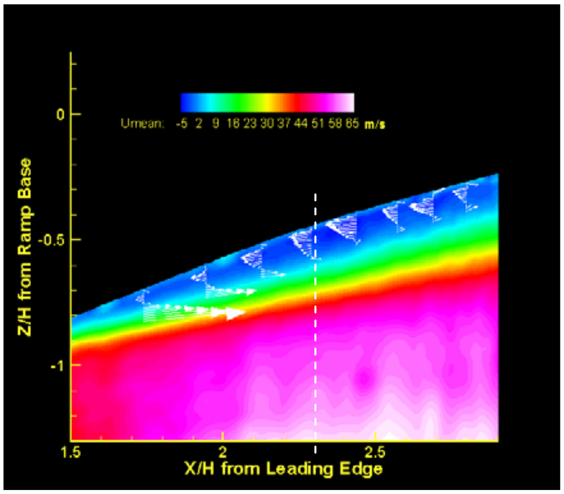

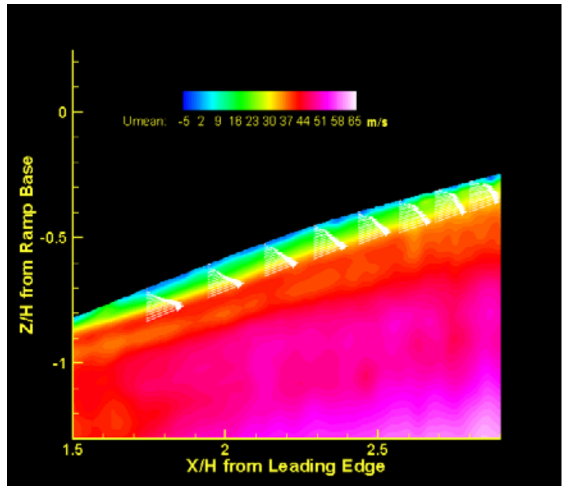

Fig. 15- a) Streamwise velocity data @65m/s: No Control

b) Streamwise velocity data @65m/s: MJ4; 90°; 10psig

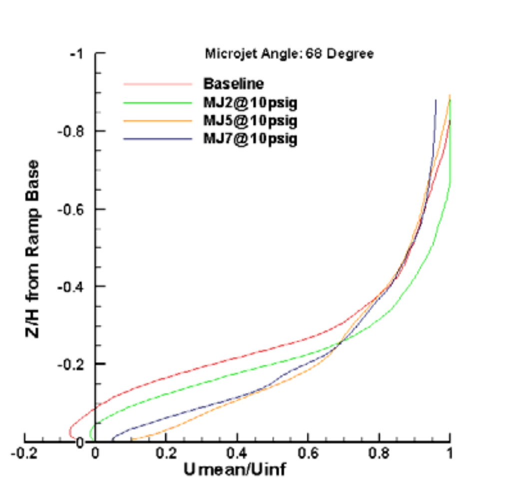

Fig. 16- Effect of Parametric variation (Location, Angle, Pressure) on mean velocity profiles X/H=2.3, U = 40 m/s, Ramp angle = 5° for MJ2, MJ5, MJ7; 68°; 10psig